2-1-2001

Adsorption and decomposition of nickelocene on Ag(100): a high-resolution electron energy loss spectroscopy and temperature programmed desorption study

D. L. Pugmire
University of Nebraska - Lincoln, pugmire@ornl.gov

C. M. Woodbridge
University of Nebraska-Lincoln, cwoodbridge@ggc.edu

N. M. Boag
Department of Chemistry, Salford University, Salford M5 4WT, UK

Marjorie Langell
University of Nebraska - Lincoln, mlangell1@unl.edu

Published in *Surface Science* 472:3 (February 1, 2001), pp. 155-171; doi:10.1016/S0039-6028(00)00939-0 http://www.sciencedirect.com/science/journal/00396028

Submitted August 4, 2000; accepted October 24, 2000; published online February 5, 2001.

Adsorption and decomposition of nickelocene on Ag(1 0 0): a high-resolution electron energy loss spectroscopy and temperature programmed desorption study

D. L. Pugmire[a], C. M. Woodbridge[a], N. M. Boag[b], and M. A. Langell[a]

[a] *Department of Chemistry and Center for Materials Research and Analysis, University of Nebraska–Lincoln, Lincoln, NE 68588-0304, USA*

[b] *Department of Chemistry, Salford University, Salford M5 4WT, UK*

* *Corresponding author. Email:* mlangell@unlserve.unl.edu

Abstract: Nickelocene adsorption and decomposition on the Ag(1 0 0) surface were studied with temperature programmed desorption and high resolution electron energy loss spectroscopy. At monolayer coverages on the relatively inert Ag(1 0 0) surface at 175 K, nickelocene physisorbs molecularly, with its molecular axis perpendicular to the surface plane. Nickelocene begins decomposing to adsorbed cyclopentadienyl and nickel at 225 K. Molecular desorption is only observed from multilayer material, at 210 K, or from the first monolayer if adjacent surface sites for decomposition are not available. The cyclopentadienyl decomposes through disproportionation to cyclopentadiene, which desorbs, and adsorbed nickel and carbon fragments on the Ag(1 0 0) surface with a maximum at 525 K.

Keywords: Electron energy loss spectroscopy (EELS), Thermal desorption, Silver

1. Introduction

Metallocenes have found uses in a wide variety of chemical and industrial applications since their discovery in 1951. Ferrocene is used as an anti-knock additive in motor fuels [1], as well as a catalyst in reactions such as the commercially important production of polyethylene [1]. Metallocene derivatives can also serve as monomer units for production of various metallocene polymers and copolymers [1]. Recently, interest has been spurred by their proposed application as sources for metallization [2] particularly by chemical vapor deposition methods [3–16].

There are several constraints placed on a material in order for it to be an effective source for the selective-area deposition of metal where the selectivity is controlled by electron or photon stimulated deposition. The material serving as the metal-source must desorb molecularly from the surface in the absence of incident radiation to ensure deposition in desired areas only. In the case of metal deposition from organometallic precursors, where organic ligands are used to volatilize the metal for transport

to the substrate, the unbound ligands should be stable and easily desorbed both in the substrate material and on the deposited metal. If they do decompose on the substrate, their decomposition products should desorb cleanly under mild conditions. This will allow for production of contaminant-free metal features.

Nickelocene has many favorable properties that give it good potential as a viable CVD and selective-area CVD source. It is less toxic than many of its alkyl counterparts and is much less toxic than nickel tetracarbonyl [12], which is commonly used for CVD of nickel. Furthermore, nickelocene is a solid at room temperature, making it easy to handle and purify, and is stable to 573 K in an inert atmosphere. Room temperature vapor pressure of this metallocene is sufficient to allow effective transport of the source material to the substrate [8].

Metallocenes have been studied as sources for both thin film production by CVD and small-metal device fabrication by selective-area CVD. For example, nickel has been deposited by pyrolysis of nickelocene over wide substrate areas to produce thin films with uniform coverage [4, 12–16]. Nickel has also been deposited in microscale patterns on silicon [3 and 5], silver [7], and copper [7] with photo or electron assisted decomposition. In one report, scanning transmission electron microscopy was used to deposit Ni from nickelocene in 10 nm wide lines on a thin-carbon film [7], demonstrating that very fine control over spatial deposition can be exercised. When information on the composition of the nickel-deposited surface has been reported, use of nickelocene in CVD processes generally has been observed to include some carbon contamination within the metal film, except in the case of threshold photolysis [7].

While a number of studies has been reported on metal deposition using metallocenes as precursors, very little is known about the surface chemistry of metallocenes at the molecular level [2, 6, 7, 17–22]. Furthermore, only a handful of studies have focused on nickelocene [7, 17–19]. A good understanding of the metallocene surface properties is necessary in order to maximize the controllability of decomposition, minimize contamination, and tailor precursors and conditions to optimum deposition efficiency. A very important piece of information in the understanding of nickelocene surface chemistry is the role that substrate reactivity plays. What effects do surface reactivity play on the thermally induced metal–ligand bond cleavage of adsorbed nickelocene? Does surface reactivity affect the fragmentation, if any, of the cyclopentadienyl ligand? What is the ultimate fate of the adsorbed cyclopentadienyl, or of its decomposition fragments? This paper presents our work on the adsorption and subsequent decomposition of nickelocene on the relatively inert Ag(1 0 0) surface, the first in a series to determine the effects of surface reactivity on nickelocene surface chemistry.

2. Experimental

A silver single crystal (Goodfellow, oriented to ±0.5° of the (1 0 0) plane) was mounted on a sample manipulator capable of resistive heating, and cooling with a liquid-nitrogen reservoir. Sample temperature was monitored with a type-K thermocouple (chromel–alumel). Surface analysis was performed in a stainless steel bell jar with a typical base pressure of 2×10^{-10} Torr. The bell jar was equipped with instrumentation to perform Auger electron spectroscopy (AES), X-ray photoelectron spectroscopy (XPS), temperature programmed desorption (TPD), and high-resolution electron energy loss spectroscopy (HREELS).

The sample was cleaned by repeated cycles of Ar^+ sputtering (0.5 keV and 10 μA) at 425 K for 10 min followed by vacuum annealing at 673 K for 20 min. This cycle was continued until the substrate surface was free of contamination, as determined by AES. All nickelocene thin films studied were prepared by exposure of the Ag(1 0 0) sample to nickelocene at 175 K, unless otherwise specified. The clean surface was dosed by admission of nickelocene (Aldrich, > 97%) vapor into the chamber through a standard leak valve equipped with a needle doser that concentrated the vapor in the vicinity of the sample surface. Exposures are reported in Langmuirs ($1L = 10^{-6}$ Torr s), and details of the doser time to Langmuir calibration procedure can be found elsewhere [20].

The high-resolution electron energy loss spectra were obtained with a LK2000 spectrometer (LK Technologies). Electrons were incident to the surface at 60° from the surface normal with a primary beam energy of 3.77 eV, and the sample current was typically 75 pA. Resolution (FWHM) of the spectra presented range from 30 to 40 cm^{-1}. Mass spectral intensities were monitored for TPD with a UTI 100C quadrupole mass spectrometer using an ionization energy of 77 eV. The mass spectrometer was equipped with a shield to minimize the detection of desorbing species from objects other than the substrate. A heating ramp of 4 K s^{-1} was used for all TPD spectra, unless otherwise noted. XPS was performed with MgKα radiation (1253.6 eV) and a Physical Electronics model 15-225G double pass cylindrical mirror analyzer. Pass energies used are reported in the XPS figure caption. The binding energies were calibrated by reference to the substrate $3d_{5/2}$ transition, taken to have a value of 367.9 eV.

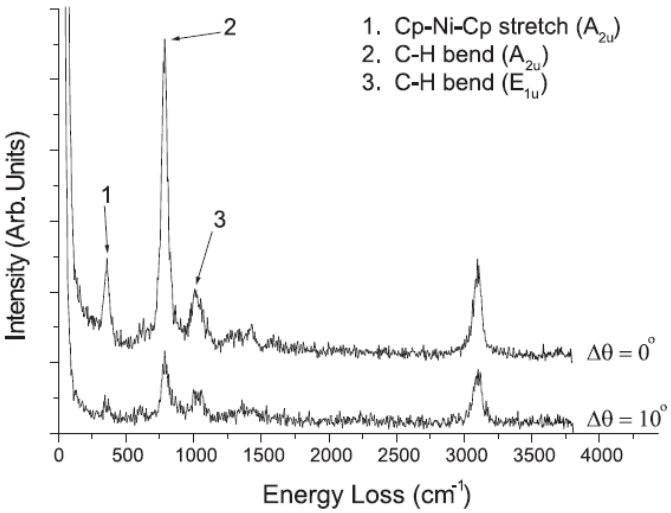

Figure 1. The on- and off-specular HREEL spectra for one monolayer (10 L) of nickelocene on Ag(1 0 0) at 175 K. Modes with A_{2u} symmetry are dipole active, and modes of E_{1u} symmetry are weak or are not observed, indicating that at coverage near one monolayer, nickelocene adsorbs with its molecular axis nearly perpendicular to the surface.

3. Results

3.1. Evidence for molecular adsorption

On the relatively inert Ag(1 0 0) surface, nickelocene is known to adsorb molecularly at temperatures of ≤ 175 K. We have previously characterized this low-temperature Ag(1 0 0)–$NiCp_2$ adsorbate for monolayer to multilayer coverages [20, 21] with XPS and HREELS and have demonstrated that nickelocene adsorbs in a layer-by-layer manner at 175 K, with the first monolayer saturating after 10 L, the second after 25 L, and multilayer thin-film formation thereafter. Several other groups [7, 17, 19] have also studied the Ag(1 0 0)–$NiCp_2$ adsorbate system, using a variety of techniques, and are in general agreement with the molecular adsorption results.

The on- and off-specular HREEL spectra for one monolayer (10 L) of $NiCp_2$ on Ag(1 0 0) at 175 K are shown in Figure 1 and their assignments summarized in Table 1. Losses are observed at 359, 784, 1013, 1431, and 3098 cm^{-1} and compare well to fundamentals reported in the IR spectrum [23]. Additional modes observed at 610 and 1588 cm^{-1} are attributed to a combination band and double loss, as discussed later in the bilayer HREELS assignments. The similarity of the HREELS loss energies to those observed in solution [23] and solid [24] IR data indicates molecular adsorption of the metallocene with no dissociation or significant rehybridization of the adsorbate molecular bonds.

In further support of the vibrational assignments made for the HREELS data and to aid in the nickelocene decomposition studies, the vibrational spectrum of adsorbed $Ni(C_5D_5)_2$ is also reported. The HREEL spectrum of Ag(1 0 0) exposed to 10 L d_{10}-$NiCp_2$ is compared to a 10 L spectrum of Ag(1 0 0)–$Ni(C_5H_5)_2$ in Figure 2. Assignments and isotope shift ratios are given in Table 1. For the molecularly adsorbed monolayer, the C–H, C–C, and ring-metal modes have υ_H/υ_D ratios of 1.33, 1.09, and 1.03, respectively, in good agreement with values observed by IR spectroscopy for $Ni(C_5H_5)_2/Ni(C_5D_5)_2$ solids [24]. The HREELS absolute energy values are also similar in magnitude to those observed in IR data [23, 24].

HREELS can be used to determine the molecular orientation using dipole-selection rules and

Table 1
Assignments of vibrational losses observed in HREELS spectra[a]

	IR of $NiCp_2$[b] solution	$Ni(C_5H_5)_2$		10 L $Ni(C_5D_5)_2$	υ_H/υ_D monolayer adsorbate	υ_H/υ_D solid[c]
		25 L	10 L			
R-M-R bend	125	138				
Ag–C stretch						
R-M-R stretch	355	364	359	349	1.03	1.05
Comb. band[d]		605	610			
C–H bend(⊥)	773	781	784	590	1.33	1.33
C–H bend(∥)	1000	1003	1013	762	1.33	1.30
C–C stretch	1430	1421	1431	1318	1.09	1.01
Double loss[e]	1545	1583	1588			
Comb. band[d]	1670	1682				
Comb. loss[f]	1773	1794				
C–H stretch	3075	3103	3098	2321	1.33	1.31[g]

[a] All energies reported in cm^{-1}.
[b] Data from Ref. [23].
[c] Data from Ref. [24].
[d] Combination band. Discussed in text.
[e] Double loss to the C–H bend (⊥) at 773 cm^{-1}.
[f] Combination loss to the C–H bend (⊥) at 773 cm^{-1} and C–H bend (∥) at 1000 cm^{-1}.
[g] Value for $FeCp_2$ from Ref. [23].

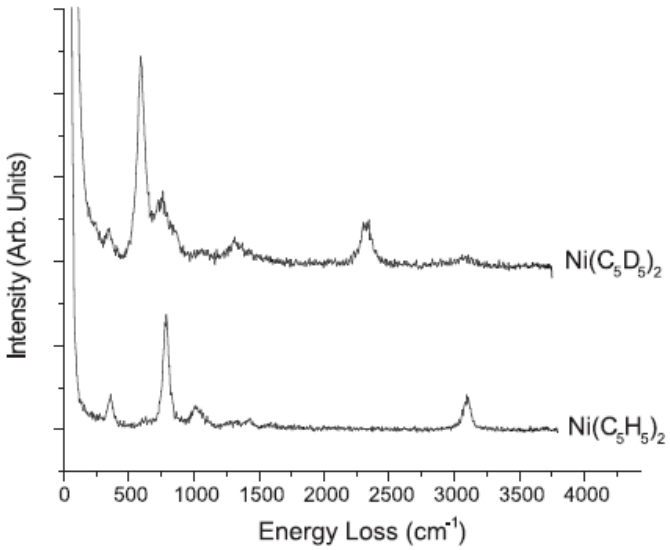

Figure 2. The HREEL spectra of monolayers for $Ni(C_5D_5)_2$, top spectrum, and $Ni(C_5H_5)_2$, bottom spectrum, on Ag(1 0 0) at 175 K.

vibrational symmetries. Molecularly adsorbed nickelocene is assumed to have its Cp rings in the staggered conformation in accordance with 100–298 K crystal structure data [25]. This conformation results in an idealized D_{5d} symmetry of the molecule if the perturbation of the surface is ignored for labeling purposes. Under this point group, modes with A_{2u} or E_{1u} symmetry are IR active. A mode with A_{2u} symmetry gives rise to a transition dipole along the *z*-axis, or Cp–Ni–Cp molecular axis, of the nickelocene. Modes with E_{1u} symmetry contain dipoles oriented in the *x*, *y* plane, or parallel to the cyclopentadienyl rings. These modes can potentially give rise to quite intense, dipole-active HREELS features, depending on the molecular orientation with respect to the substrate surface. A weakly adsorbed nickelocene molecule will have four vibrations active and polarized along the molecular axis. There are also six IR active modes polarized in the *x*, *y* plane of the molecule. Four modes in particular, two A_{2u} and two E_{1u}, are helpful in determining the adsorbed metallocene orientation. The atomic motions of these four IR active modes are shown in Figure 3.

If the molecule adsorbs with its molecular axis perpendicular to the surface plane (along the surface normal), the A_{2u} modes are expected to be dipole active and the E_{1u} modes are not. At the other extreme, if the metallocene adsorbs so that the cyclopentadienyl rings are perpendicular to the surface, only the E_{1u} modes will be dipole active. With the molecule adsorbed at any angle

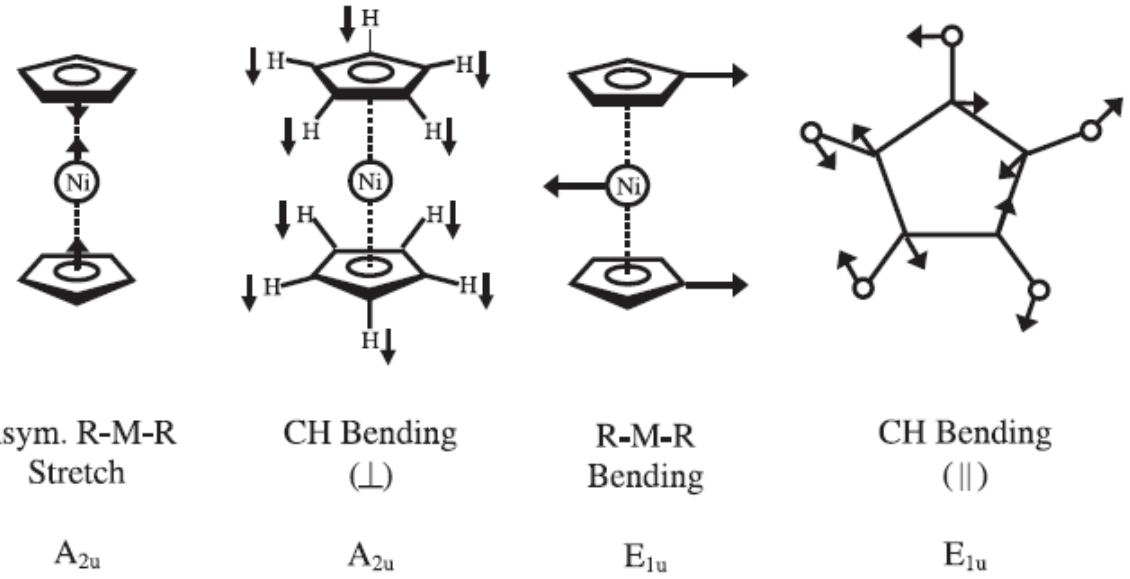

Figure 3. The atomic motions of the four vibrational modes relevant to nickelocene orientation determination, and their symmetries. Modes of A_{2u} symmetry are IR active and polarized along the molecular axis. Modes with E_{1u} symmetry are polarized in a plane parallel to the cyclopentadienyl ring planes.

between these extremes, both the A_{2u} and E_{1u} modes can exhibit dipole scattering.

In the nickelocene monolayer spectrum, shown in Figure 1, the asymmetric ring-metal-ring stretch and asymmetric C–H bend (⊥), both of which have A_{2u} symmetry, appear as intense modes at 359 and 784 cm^{-1}, respectively. Modes with E_{1u} symmetry appear weaker in intensity, for example the asymmetric C–H bend (||) at 1013 cm^{-1}, or in some cases are not observed at all. A comparison with the corresponding off-specular data in Figure 1 shows a substantial loss in intensity for all modes of A_{2u} symmetry but not for modes of E_{1u} symmetry, indicating that only the former are dipole active. This indicates that at exposures corresponding to approximately one monolayer, the majority of the adsorbed monolayer is oriented with its molecular axis perpendicular to the plane of the surface [19–21].

Figure 4 shows the on- and off-specular HREEL spectra for a 25 L exposure of nickelocene to the Ag(1 0 0) surface, corresponding to approximately two monolayers. The energies observed in these spectra are very similar to those observed in solution [23] and solid [24] nickelocene IR data, again indicating molecular adsorption. For completeness, a full assignment of the vibrational spectrum of molecularly adsorbed nickelocene

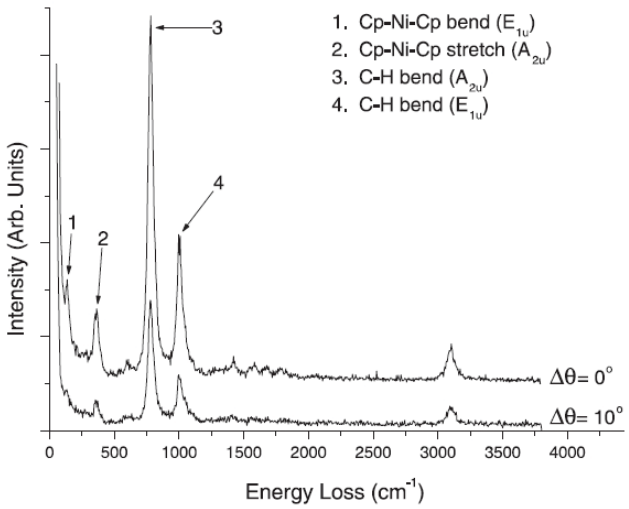

Figure 4. The on- and off-specular HREEL spectra for a bilayer (25 L) of nickelocene on Ag(1 0 0) at 175 K. Modes of both A_{2u} and E_{1u} symmetry are dipole active, indicating that at this coverage, nickelocene is oriented with its molecular axis canted with respect to the surface normal.

is included in Table 1 since these data have not previously been reported in entirety. The most intense losses are found at 138, 364, 781, 1003, 1421, and 3103 cm^{-1} and compare well to fundamentals observed in the IR spectrum [23, 24].

Additional losses are observed at 605, 1583, 1682, and 1794 cm^{-1}. These modes cannot be attributed

to fundamentals of nickelocene, as there are no predicted fundamentals with similar energies [23 and 24]. The modes at 1583 and 1794 cm^{-1} are double losses, 2 × 781 cm^{-1} (C–H bend ⊥) and 781 + 1003 cm^{-1} (C–H bend ||), respectively. These modes are not due to overtones or combinations, as they would have symmetries incompatible with the dipole activity observed, but actually occur through two sequential scattering events. The remaining two losses can be attributed to combination bands. The combination of symmetric and asymmetric ring-metal-ring stretches has an energy of 575 cm^{-1} and A_{2u} symmetry. The loss at 1682 cm^{-1} can be attributed to the combination of C–C and C–H modes with E_{1u} symmetry, which have been observed in the IR spectra of metallocenes at similar energies [23, 24].

As the detection angle is changed to 10° off-specular (Figure 4), the spectrum undergoes a sharp drop in intensity for the ring-metal-ring bend and C–H bend (||) at 138 and 1003 cm^{-1}, both of which have E_{1u} symmetry, indicating that the modes are dipole active. The asymmetric ring-metal-ring stretch and C–H bend (⊥) modes at 364 and 781 cm^{-1} posses A_{2u} symmetry, and are also dipole active. The high intensities and dipole activity of both the E_{1u} and A_{2u} modes indicate that adsorbed nickelocene has become canted with respect to the surface at bilayer coverages. The tilting had previously been observed for multilayer ($\lesssim$ 5 ML) nickelocene thin films [19, 20 and 21] and is here demonstrated conclusively to occur as early as the second layer (2 ML).

XPS measurements of multilayer nickelocene yield binding energies of 284.6 eV for the C 1s transition and 854.6 and 871.7 eV for the Ni $2p_{3/2}$ and $2p_{1/2}$ transitions, respectively, in good agreement with literature values for molecular nickelocene [26]. C 1s and Ni 2p XPS data for a one monolayer film show binding energies indistinguishable from those obtained for the multilayer nickelocene condensate. The C 1s/Ni 2p intensity ratio for the $NiCp_2$ monolayer is 0.35, which correlates well with the expected 10/1 C/Ni atomic ratio when differences in the relative XPS cross-sections are taken into account [27]. Thus, the XPS results are compatible with molecular adsorption.

Information on absolute nickelocene surface concentrations can be obtained from the C 1s and Ag 3d XPS peak intensities. Assuming an exponential attenuation of electrons with depth [28], the relationship for the intensities at one monolayer coverage is given by:

$$\frac{I_C}{I_{Ag}} = \frac{E_{k,Ag}^{1/2} C_C \sigma_C}{E_{k,C}^{1/2} C_{Ag} \sigma_{Ag} I_{0,Ag} \exp\left(\frac{-d_{NiCp_2}}{\lambda_{NiCp_2} \cos(\theta)}\right)} \quad (1)$$

where

$$I_{0,Ag} = \sum_{n=0}^{\infty} \exp\left(\frac{-n d_{Ag}}{\lambda_{Ag} \cos(\theta)}\right) \quad (2)$$

$E_{k,C}$ and $E_{k,Ag}$ are photoelectron kinetic energies for carbon 1s and silver $3d_{5/2}$ respectively, C_C and C_{Ag} are carbon and silver surface concentrations, σ_C and σ_{Ag} are photoionization cross-sections for the respective transitions, d_{NiCp2} and d_{Ag} are the nickelocene and silver layer thicknesses, λ_{NiCp2} and λ_{Ag} are the mean free paths of an 885 eV Ag $3d_{5/2}$ electron passing through nickelocene and Ag, respectively, and θ is the photoemission detection angle.

The C 1s/Ag 3d intensity ratio for nickelocene on Ag(1 0 0) was measured at an exposure corresponding to one monolayer, yielding a ratio of 0.024, very similar to the value observed for ferrocene adsorption on the same surface [29]. This ratio was used in Equation (1) to estimate the monolayer coverage of nickelocene. Values for other parameters in the equation are: $E_{k,C}$ = 969.0 eV, $E_{k,Ag}$ = 885.7 eV, σ_C = 1.00 (× 22000 barns) [27], σ_{Ag} = 18.04 (× 22000 barns) [27], d_{NiCp2} = 7.33 [25, 30], d_{Ag} = 2.89 [22], $\lambda_{NiCp2} \equiv \lambda_{Ag}$ = 11.8 [31], and θ = 41° [32]. This gives a C/Ag atomic concentration ratio of 0.7, or 0.07 nickelocene molecules per silver surface atom. A similar analysis using the observed Ni 2p/Ag 3d ratio of 0.068 gives a Ni/Ag atomic concentration ratio of 0.06. These concentration ranges are reasonable for monolayer coverage, and are very similar to that observed for ferrocene [29]. The XPS data indicate ~14 silver atoms per $NiCp_2$ molecule, suggesting an extremely open, low density packing of metallocene. Hexagonal closest packing of nickelocene molecules

idealized as cylinders with a surface footprint set by the van der Waal diameters of Cp rings gives a ratio of 3 silver atoms for every molecule, or a C/Ag intensity ratio of 0.11.

Mean free paths of electrons through organometallic compounds have not been well documented. The mean free path used for the electron through the nickelocene monolayer in Equation (1) was approximated in the calculation above by setting it equal to the mean free path used for silver. In lieu of other information, this is a reasonable approximation, as electrons generally have similar mean free paths through different materials [33] and previous studies on ferrocene have suggested that the mean free path is close to that of silver at 885 eV [29]. However, there is some indication that the mean free paths for organic materials can be longer than those for metals, depending on the kinetic energy of the electron and the material [34]. For this reason, surface concentrations were also calculated using an upper limit on the mean free path by assuming that the relatively open nickelocene overlayer does not attenuate the Ag 3d photoelectrons, effectively setting the mean free path to be infinite. Even with this extremely large mean free path of the electron through the metallocene the film density is predicted to be lower than that of a complete closest-packed layer at 6–7 silver atoms per nickelocene.

The XPS and HREELS data presented above indicate molecular adsorption to be the primary mode of nickelocene adsorption at all coverages; accordingly, molecular nickelocene is also observed in TPD. This is shown in Figure 5 for TPD spectra from the $NiCp_2$ bilayer (25 L) in which signal for the following ions are reported: $C_2H_2^+$ (m/q = 26), $C_3H_3^+$ (m/q = 39), $C_5H_5^+$ (m/q = 65), Ni^+ (m/q = 58), $NiC_3H_3^+$ (m/q = 97), $NiCp^+$ (m/q = 123), and $NiCp_2^+$ (m/q = 188). Ni-containing fragments are plotted as solid lines, while fragments not containing Ni are displayed as dashed lines. The concurrent appearance of all expected fragments, including the $NiCp_2^+$ parent ion, in the low temperature region (< 300 K), indicates that these peaks are due to the molecular desorption of nickelocene from the surface and arise from fragmentation of the parent molecule in the mass spectrometer ionizer.

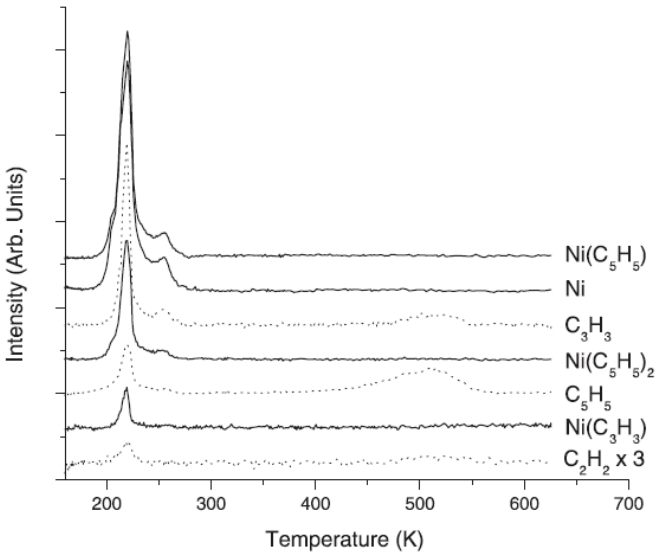

Figure 5. Multiplexed thermal desorption data for a bilayer (25 L) of nickelocene from Ag(1 0 0) with a heating rate of 2 K s^{-1}. The solid traces indicate nickelocene fragments containing nickel, while the dashed traces indicate fragments containing C and H only. The low temperature features (200–300 K) are apparent in all spectra, indicating molecular desorption in this temperature region. The high temperature feature (~525 K) is not observed for any nickel-containing fragment, indicating it is not due to desorption of molecular nickelocene.

However, molecular desorption does not explain the origin of the broad peak found at higher temperatures and which is only observed for nickel-free fragments of m/q = 66 or less. As will be shown below, this TPD feature arises from adsorbed Cp ligands that are produced when molecularly adsorbed nickelocene dissociates upon heating. The absence of this feature in the high temperature regions of TPD from nickel-containing ions clearly indicates that desorption in this region is due to adsorbate fragments and not from molecularly adsorbed nickelocene.

3.2. Decomposition of adsorbed nickelocene

In order to further investigate the decomposition products and mechanisms of nickelocene surface chemistry on Ag(1 0 0), the TPD spectrum of the Cp fragment (m/q = 65) was monitored as a function of exposure (Figure 6). At submonolayer coverages of < 0.5 ML (< 5 L) no molecular nickelocene desorption is detected in the TPD; only the ligand fragment peak, labeled D in Figure 6, is

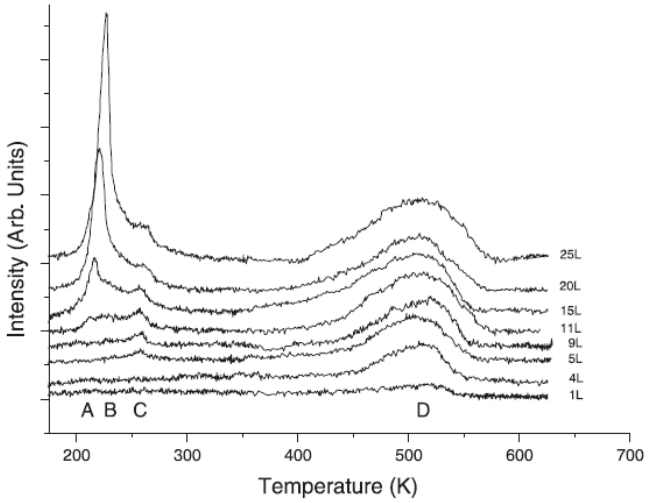

Figure 6. TPD spectrum of m/q = 65 ($C_5H_5^+$) as a function of nickelocene exposure. Peak D is apparent at lower coverages, and peaks C, B, and A grow in with higher exposure.

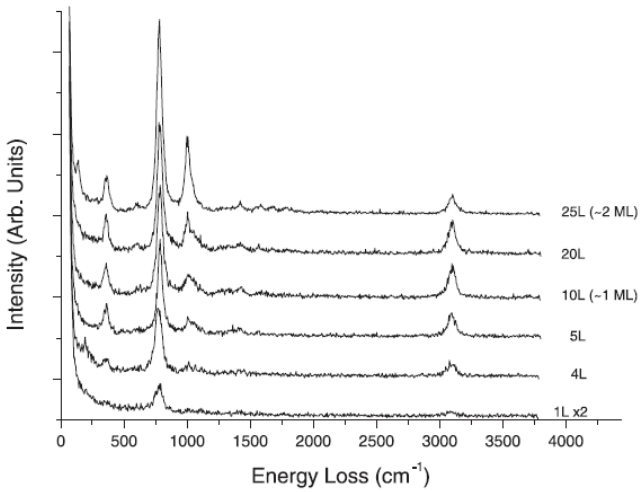

Figure 7. The HREEL spectrum of nickelocene on Ag(1 0 0) at 175 K as a function of exposure. Adsorption of 5 L or greater results in molecular adsorption, while lower coverages show partial decomposition to adsorbed cyclopentadienyl.

observed. This peak is due to the disproportionation of free cyclopentadienyl adsorbate ($C_5H_{5\ ads}$) on the Ag(1 0 0) surface into cyclopentadiene (C_5H_6) and cyclopentadienyl fragments, as will be shown below. Peak D has a maximum at 525 K and increases in intensity with exposure until it saturates at approximately 10 L, the saturation exposure for the first monolayer of nickelocene.

It is only with exposures greater than or approximately equal to 5 L that desorption features attributable to molecular nickelocene desorption first appear in TPD. At 5 L, a peak due to molecular desorption, labeled C, is found with a maximum at 255 K. The intensity of peak C increases with increasing exposure up to approximately 10 L but the peak maximum does not shift in temperature, indicating first-order desorption. At approximately 10 L, a second, broad, molecular desorption feature appears, peak B in Figure 6, with a maximum desorption temperature of 225 K. At 11 L, a third peak, labeled A, due to molecular desorption grows in with an initial desorption maximum of 210 K. The intensity of this peak does not saturate and continues to grow and shift to higher temperature as the exposure of the surface to nickelocene is increased, indicating the zero-order kinetic behavior observed for multilayer desorption.

To aid in the understanding of the mechanism that gives rise to the TPD features, HREELS data were obtained as a function of coverage and of annealing temperature. The HREEL spectrum of nickelocene on Ag(1 0 0) at 175 K is shown as a function of exposure in Figure 7. At bilayer coverage, the spectrum indicates that the molecular axis of nickelocene is canted with respect to the surface normal, as discussed above. Decreasing the coverage below 2 ML correlates with a decrease in intensity of the modes polarized within the planes of the Cp rings as the nickelocene adopts an upright orientation at these lower coverages (0.5–1 ML). However, all these data give evidence of molecularly adsorbed nickelocene only.

At coverages of less than one-half monolayer (<5 L), additional HREELS losses are observed that cannot be correlated with molecularly adsorbed nickelocene, regardless of the molecular tilt angle assumed. These loss peaks have been observed even at substrate temperatures as low as 140 K. A mode now appears at 202 cm^{-1} along with a low energy shoulder on the C–H bend ($\perp$) at 772 cm^{-1}. These extra, non-molecular loss features result from free cyclopentadienyl ligand adsorbates (C_5H_{5ads} = Cp_{ads}) that have dissociated from $NiCp_2$ on the silver surface and their method of production is made clear from analysis of the HREEL spectrum as a function of annealing temperature.

Figure 8 shows the effects on the HREEL spectrum of annealing molecularly adsorbed nickelocene

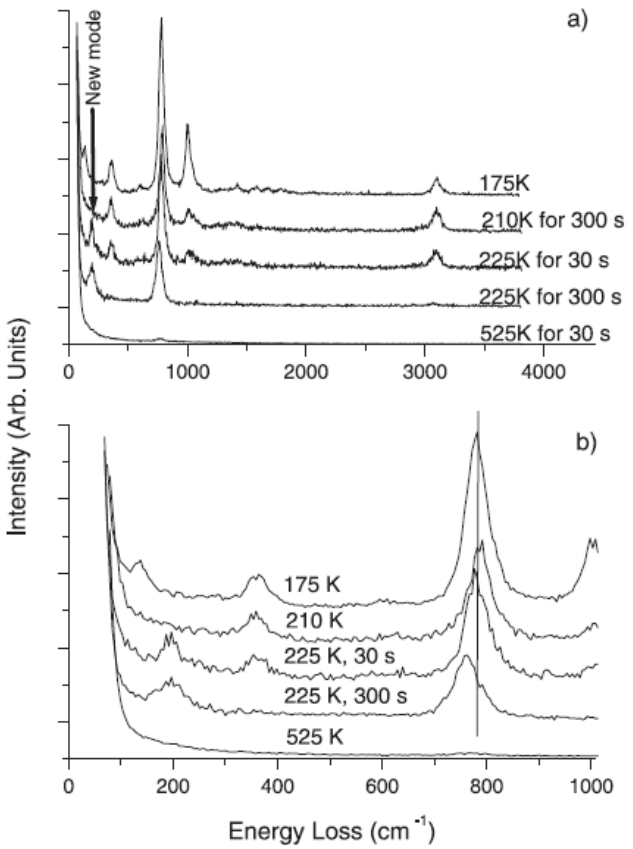

Figure 8. (a) The HREEL spectra of a bilayer (25 L) of nickelocene on Ag(1 0 0) annealed to temperatures corresponding to features observed in TPD data. Appearance of the 197 cm^{-1} mode at 225 K indicates decomposition to cyclopentadienyl. (b) Enlargement of the low energy loss region clearly shows a shift of the C–H bend (⊥) to lower energy at higher temperatures.

for a Ag(1 0 0) surface dosed with 25 L of $NiCp_2$. A significant change is observed upon annealing the surface at 210 K for 300 s. This temperature corresponds to multilayer desorption (peak A) in the TPD data. The intensities of the modes with E_{1u} symmetry have now decreased significantly, leaving a spectrum very similar to that of the monolayer (10 L) exposure spectrum. This similarity and the lack of saturation of peak A in the TPD spectrum with increasing exposure confirm that the desorption feature is due to multilayer desorption, including desorption of the second layer. Furthermore, as expected for a multilayer desorption temperature, heating a submonolayer film to 210 K does not affect the HREEL spectrum.

Peak A of the thermal desorption data was analyzed using the zero order, leading-edge method [35] in which the natural log of the desorption rate is plotted versus the inverse of the temperature. Multiplying the slope of the least-squares linear fit by $-R$ yielded a desorption energy of 21 ± 2 kcal mol^{-1} for multilayer nickelocene. This can be compared to a heat of sublimation of 17.1 ± 0.2 kcal mol^{-1} [36].

When the surface is annealed to 225 K, a temperature corresponding to peak B in the thermal desorption spectrum, for 30 s a new mode appears at 197 cm^{-1} in the HREEL spectrum (Figure 8) and the asymmetric C–H bend (⊥) shifts to lower energy at 762 cm^{-1}, very similar to the additional peaks found in the low coverage, 175 K spectra shown in Figure 7, that were not attributable to molecularly adsorbed nickelocene. An even more dramatic change in the HREEL spectrum is observed upon annealing the surface at 225 K for longer times. Modes attributed to molecularly adsorbed nickelocene are no longer apparent after approximately 300 s. The losses first appearing in the 225 K short anneal (30 s) data are now the dominant features in the spectrum . Additionally, the C–H stretching loss is now centered at 3074 cm^{-1}, and has lost considerable intensity. This HREEL spectrum is also obtained when similar coverages on the Ag substrate are heated to 255 K for 30 s (not shown), or flashed to 275 K (not shown), which correspond to the maximum of peak C and just beyond peak C in the desorption data.

The simplicity of the HREEL spectrum from molecularly adsorbed nickelocene after it has been annealed to 225 K suggests decomposition to an adsorbed species with high symmetry. A likely product of nickelocene decomposition is an adsorbed cyclopentadienyl species, as has previously been observed for ferrocene decomposition [37] and is shown schematically in the following:

$$NiCp_{2ads} \rightarrow Ni_{ads} + 2Cp_{ads}$$

The high D_{5h} symmetry of the cyclopentadienyl anion results in four IR active fundamentals: a C–H bending (⊥) mode polarized perpendicular to the plane of the ring, and a C–H bending (||), C–H stretching, and C–C stretching mode polarized

Table 2
Assignments of vibrational losses observed in HREELS spectra of adsorbed Cp and comparison to adsorbed nickelocene[a]

	Cp on Ag(1 0 0)				$NiCp_2$ on Ag(1 0 0) υ_H/υ_D ($NiCp_2$)
	Cp on Ag(1 0 0)[b] (cm^{-1})	C_5H_5 on Ag(1 0 0) (cm^{-1})	C_5D_5 on Ag(1 0 0) (cm^{-1})	υ_H/υ_D (Cp)	
Ag-R stretch	<270	197	192	1.03	1.03[c]
C–H(D) bend	760	762	561	1.36	1.33
C–H(D) stretch	N.R.	3074	2301	1.34	1.33

N.R. = Not reported.
[a] Cp films obtained by annealing molecular $NiCp_2$ films to 225 K.
[b] Data from Ref. [37].
[c] Value of metal-ring stretch in $NiCp_2$.

parallel to the plane of the ring. The 197, 762, and 3074 cm^{-1} modes observed in Figure 8 are, therefore, assigned as the surface-ring stretch, C–H bending (⊥), and C–H stretch, respectively. These assignments are given in Table 2 and compared to η^5-Cp on Ag(1 0 0) [37] and d_5-Cp on Ag(1 0 0) results.

The on- and off-specular HREEL spectra of d_5-Cp, shown in Figure 9 and summarized in Table 2, were obtained from a 25 L exposure of the Ag(1 0 0) surface to $Ni(C_5D_5)_2$, and subsequent annealing at 225 K for 300 s. Energy loss ratios of 1.36 and 1.34 for C–H modes and 1.03 for the surface-ring mode

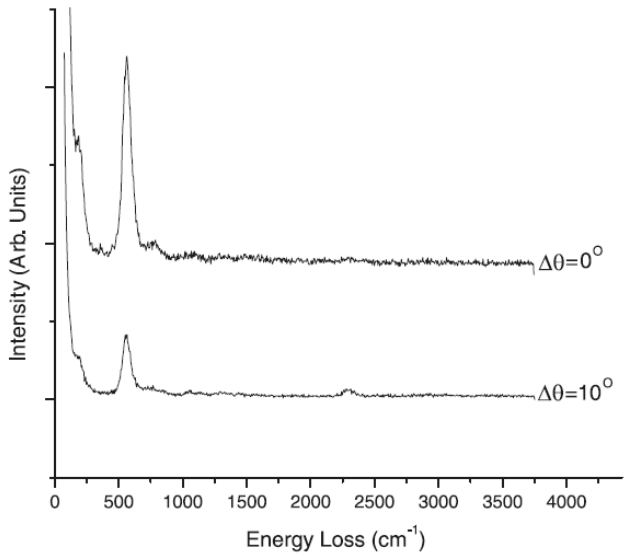

Figure 9. The on- and off-specular HREEL spectra of d_5-cyclopentadienyl adsorbed on Ag(1 0 0). Dipole activity of the Ag-ring stretch (192 cm^{-1}) and the C–D bend (⊥) (561 cm^{-1}) and low intensity of the C–D stretch (2301 cm^{-1}) indicate that the ring plane is parallel to that of the surface.

are observed, which are comparable to isotope shifts observed in molecular nickelocene above. The intensities of the surface-ring stretch at 192 cm^{-1} and the C–D bending (⊥) mode at 561 cm^{-1}, both of which are polarized perpendicularly to the plane of the anion, drop sharply in the off-specular spectrum. The three modes polarized within the molecular plane are not observed, or in the case of the C–D stretching at 2301 cm^{-1}, are observed as low intensity, dipole-inactive modes. This indicates that the plane of the adsorbed cyclopentadienyl resulting from decomposition of the metallocene is oriented parallel to the surface, similar to the Cp ring in the molecularly adsorbed $NiCp_2$ monolayer.

The changes in the HREEL spectrum (Figure 7) of very low nickelocene exposures (< 5 L) can thus be attributed to the presence of adsorbed cyclopentadienyl, resulting from decomposition of a portion of the adsorbed nickelocene. This partial decomposition is further demonstrated in Figure 10, which shows the 4 L exposure HREEL spectrum, along with a 10 L (1 ML) spectrum and an adsorbed Cp spectrum for comparison. The mode at 202 cm^{-1} and the low energy shoulder on the C–H bending at 781 cm^{-1} observed in the 4 L HREEL data are very similar to the adsorbed cyclopentadienyl spectrum obtained after annealing a monolayer of nickelocene on Ag(1 0 0) to 225 K. Any further increase in exposure, > 4 L, suppresses the adsorption mode that gives rise to the energy losses from the free-ligand cyclopentadienyl adsorbate.

Features B and C in the thermal desorption spectrum (Figure 6) are clearly due to molecular

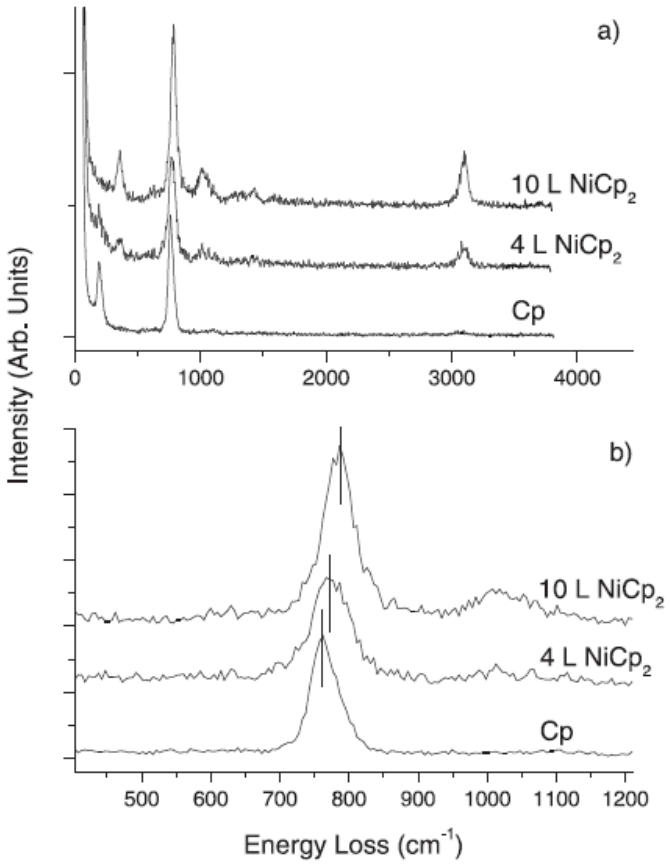

Figure 10. (a) Comparison of low coverage (4 L) nickelocene HREEL spectrum at 175 K with molecularly adsorbed nickelocene and adsorbed cyclopentadienyl, (b) 400–1200 cm^{-1} region enlargement of (a). Low nickelocene coverages result in partial decomposition of nickelocene to adsorbed cyclopentadienyl, at temperatures as low as 145 K.

desorption. However, there are several possible explanations for multiple molecular desorption features in TPD. Simplistically, peak C could result from molecular desorption from the first monolayer, and B from the desorption of nickelocene from the second monolayer. However, this is not consistent with XPS data [20] which indicate that the monolayer forms in a layer-by-layer growth mode that is not complete until 10 L exposure, at which point both B and C have appeared and saturated in the TPD spectrum. Furthermore, nickelocene decomposes slowly at 225 K, the desorption temperature maximum of peak B, but not at 210 K, the desorption temperature maximum of the multilayer peak A, indicating that this mechanism would require the unlikely result of decomposition within the second layer but not in additional multilayers, despite the fact that intermolecular interactions are comparable.

The existence of three molecular desorption temperatures could also be attributed to desorption of multilayer material (peak A) and from two different monolayer adsorbate species (peaks B and C). However, only one nickelocene species, a weakly bound, up-right molecular adsorbate, is observed in the HREELS for monolayer and submonolayer coverages, regardless of how the surface has been heated. Furthermore, the first monolayer appears to form with no detectable change in the sticking coefficient [20], indicating that if two different surface adsorbate species form, they do not appear to do so sequentially. There is, therefore, no evidence for two different molecular adsorbate states within the first monolayer.

A possibility in better agreement with the observed HREELS, XPS and TDS data is that only one molecularly adsorbed nickelocene species forms in the first monolayer, but that this species desorbs by two different mechanisms. Bilayer and higher multilayers $NiCp_2$ desorb without decomposition at 210 K (peak A). Monolayer adsorbate, however, undergoes a slow decomposition to yield free Cp ligands and nickel metal. While small amounts of decomposed metallocene are found on submonolayer (< 0.5 ML) exposure, the rate of decomposition is negligible on the 1–2 h time scale of the HREELS experiment for higher coverages at 175 K, but occurs at a detectable rate at 225 K. This can be seen in Figure 8 where significant decomposition is apparent in the HREEL spectrum for the bilayer after 30 s and appears to be complete after 300 s.

The cyclopentadienyl ligands remain bonded to the Ag(1 0 0) substrate, and for low coverages (< 0.5 ML) this presents no problem since the relatively open monolayer adsorption structure still allows for sufficient surface sites for additional decomposition products. Molecular desorption of the undecomposed nickelocene becomes a competing process to decomposition at 255 K (peak C), providing some of the undecomposed $NiCp_2$ remains on the surface to desorb at this temperature. This occurs after 4 L exposure, or approximately one-half monolayer, at a TDP heating rate

of 4 K s^{-1}. Slower heating rates (1–3 K s^{-1}) produce less of peak C and more decomposition products.

For coverages $\gtrsim$ 0.5 ML, there is insufficient room on the substrate surface to accommodate both Cp rings and the nickel metal from the nickelocene decomposition. The Ag(1 0 0)–Cp adsorbate is relatively strongly bonded, and competes quite favorably with the molecularly adsorbed nickelocene at 225 K, displacing it to produce peak B. On the time scale of HREELS and TPD measurements, both Cp rings appear to dissociate from the nickel simultaneously and there is no evidence for the presence of $NiCp_{ads}$.

It is possible to decrease the amount of desorption in peak C by pre-decomposing metallocene on the Ag(1 0 0) surface to increase the site blockage with free-ligand cyclopentadienyl adsorbate. Molecular desorption from peak C is suppressed by successive cycles of dosing at 175 K and heating to 300 K, shown in Figure 11 in a series of TPD spectra of sequential 10 L nickelocene exposures. During acquisition of these data, the surface was heated from 175 to 300 K, allowed to cool to 175 K, and dosed again. This results in an eventual near saturation of the surface with adsorbed cyclopentadienyl and nickel fragments. That complete saturation of the surface does not take place, at least after six cycles, is evident by a small peak B in the topmost trace of Figure 11.

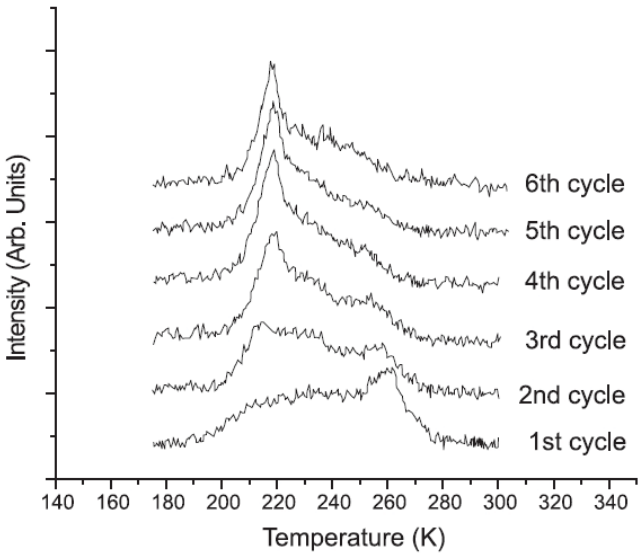

Figure 11. The $C_5H_5^+$ (m/q = 65) thermal desorption spectra from Ag(1 0 0) obtained for cycles of 10 L exposures to nickelocene followed by desorption to 300 K. As more surface adsorption sites are occupied by decomposition products adsorbed cyclopentadienyl and nickel, the amount of molecular adsorption, and consequently desorption, at the first monolayer (peak B+C) is decreased and at the second monolayer (peak A) is increased.

Repetition of dosing and heating cycles yields a surface in which most adsorption sites are occupied by nickel and cyclopentadienyl species. The low thermal mobility of cyclopentadienyl on Ag(1 0 0) [37] results in isolated, unoccupied adsorption sites, surrounded by sites occupied by Cp and nickel. Additional 10 L dosing/heating cycles result in a small amount of nickelocene being adsorbed at available surface sites, while the remainder is adsorbed in the multilayer state. Peak C diminishes in intensity because, as the surface is saturated with immobile species (Cp and nickel), fewer potential nickelocene adsorption sites remain on the substrate. The nickelocene that does adsorb, decomposes and displaces adjacent molecular nickelocene (peak B) before the desorption temperature of peak C is reached.

3.3. Decomposition of adsorbed cyclopentadienyl

Peaks A, B, and C in Figure 6 are due to molecular desorption from multilayers and the first monolayer. It has also been established that the high temperature peak, D, is not the result of molecular desorption. HREELS data indicate that upon annealing at 525 K for 30 s, corresponding to peak D in Figure 6, all vibrational features disappear except for a very low intensity mode at 767 cm^{-1}, indicating desorption or decomposition of nearly all molecular species. Peak D in the thermal desorption data cannot be due to molecularly desorbed nickelocene or to NiCp fragments because of the absence of nickel-containing species co-desorbing in the thermal desorption spectrum. HREELS data indicate the existence of adsorbed cyclopentadienyl on Ag(1 0 0) between 225 and 450 K. However, peak D cannot arise directly from Cp desorption, as this produces a negatively charged and not very stable gas phase cyclopentadienyl species ($C_5H_5^-$).

A similar situation was observed in the study of cyclopentadiene on Pt(1 1 1) [38] in which cyclopentadiene underwent partial dehydrogenation at 200 K on Pt(1 1 1) to form η^5-Cp. Heating to 400 K resulted in disproportionation to residual carbon and desorbing cyclopentadiene (C_5H_6). Therefore, $C_5H_6^+$ (m/q = 66) was monitored, along with H_2^+ (m/q = 2) (Figure 12), to determine that cyclopentadienyl hydrogenation to cyclopentadiene is occurring to produce this desorption feature. The observed ratio of m/q = 66–65 (1.4 C_5H_6/C_5H_5) for peak D is comparable to what is observed in the mass spectrum of cyclopentadiene vapor [39]. The mass 2 TPD spectrum also shown in Figure 12, indicates H_2 evolution in the same temperature region as C_5H_6 production. It is clear that the hydrogen desorption in this temperature region is reaction limited, as H_2 is observed to desorb from silver surfaces at temperatures < 200 K [40, 41]. The data are, thus, consistent with the dehydrogenation of adsorbed cyclopentadienyl to give cyclopentadiene and H_2 through a disproportionation reaction:

$$2C_5H_{5(ads)} \rightarrow C_5H_6 + 5C_{ads} + 2H_2$$

The kinetic reaction orders and activation energy of the cyclopentadiene peak can be determined by an analysis based on a modified Arrhenius plot [40]. Plots of [ln(N) − $n$ln(θ)] versus [1/T] were constructed, where $N$is the relative desorption rate, θ is the relative coverage, and n is the reaction order. Figure 13 displays the plots of n = 0.5, 1, and 2 for the desorption spectrum of a 25 L exposure of nickelocene (top spectrum of Figure 7) in the temperature region of peak D. Analysis of 10 thermal desorption spectra yielded a value of 13.9 ± 1.2 kcal mol^{-1} for the activation energy of cyclopentadienyl disproportionation. The plots were only linear for first-order kinetics, n = 1. A reaction order of one likely indicates the presence of a first-order rate limiting step, such as the dehydrogenation of cyclo-

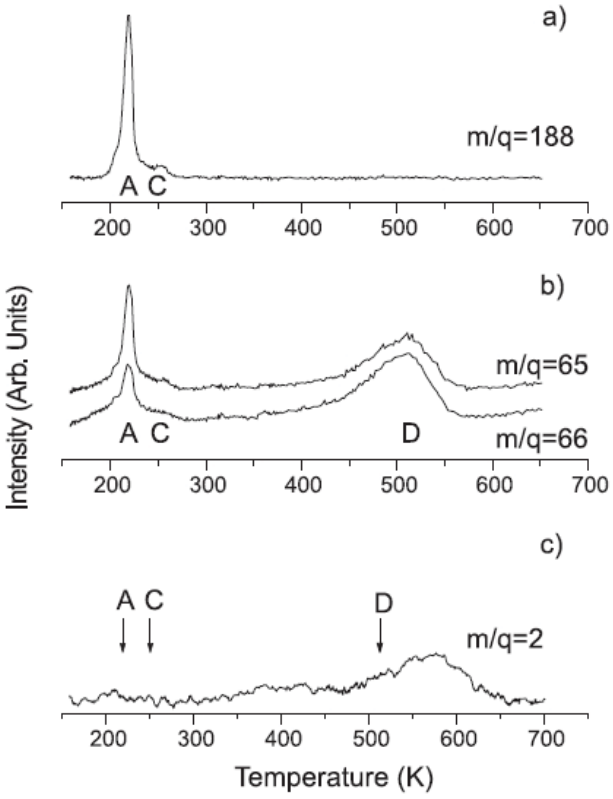

Figure 12. Multiplexed thermal desorption data for a bilayer (25 L) of nickelocene from Ag(1 0 0) with a heating rate of 2 K s^{-1}. (a) $NiCp_2^+$, (b) $C_5H_5^+$ and $C_5H_6^+$, and (c) H_2^+ showing disproportionation of adsorbed cyclopentadienyl to C_5H_6 and H_2. Labels A, C and D refer to TPD states discussed in the text. State B is obscured by multilayer state A at this coverage. The arrows in the m/q = 2 trace indicate the approximate positions of H_2 expected from nickelocene fragmentation.

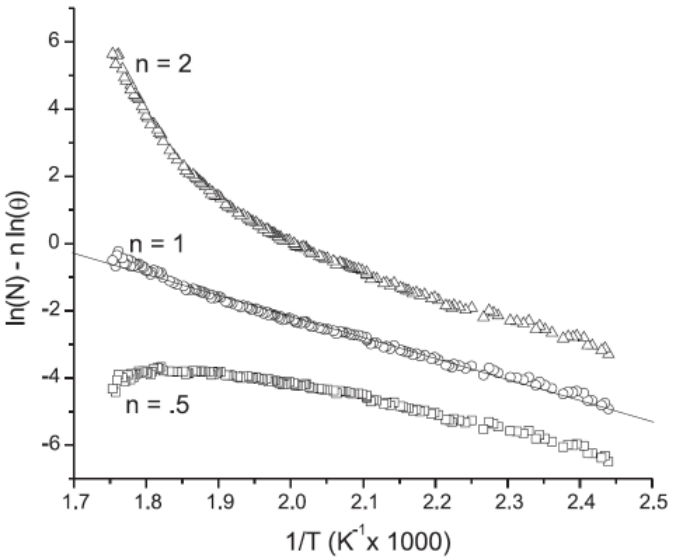

Figure 13. Arrhenius plots of varying kinetic order (n = 0.5,1,2) for the cyclopentadienyl disproportionation feature, peak D, of a 25 L exposure of the Ag(1 0 0) surface to nickelocene. The plot is only linear for a kinetic order of one, indicating a first-order rate-limiting step.

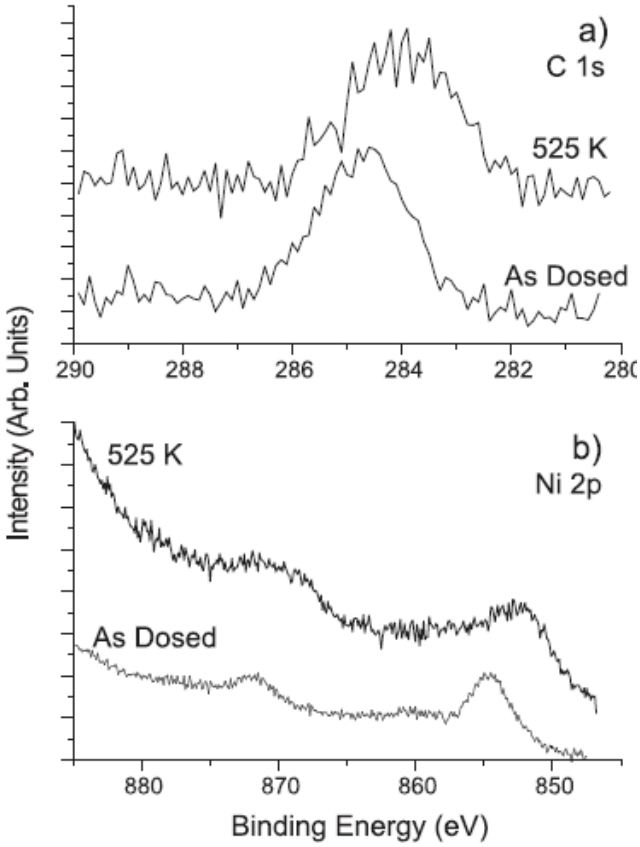

Figure 14. (a) C 1s and (b) Ni 2p XP spectra for a 25 L exposure of nickelocene to Ag(1 0 0) as dosed (top spectra) and annealed to 525 K for 30 s (bottom spectra). The presence of nickel and carbon after annealing to 525 K indicates that the surface is not returned to a pristine state.

pentadienyl. Assuming a reaction order of one, the activation energy was also calculated using the Redhead maximum rate method [42]. This yielded an average activation energy of 18 ± 4 kcal mol^{-1} for the same 10 spectra, which is within error of the value obtained with the modified Arrhenius plot.

XPS analysis of the Ag(1 0 0) surface exposed to 25 L $NiCp_2$ and annealed at 525 K for 30 s indicates that the surface is not returned to its pristine state after Cp desorption through disproportionation. The C 1s and Ni 2p regions are shown as the top spectra in Figure 14a and b, respectively, and are summarized in Table 3. These spectra were collected at pass energies of 50 eV for the C 1s and 200 eV for the Ni 2p. The C 1s photoelectrons are now observed with a binding energy of 283.9 eV. This shift to lower binding energy for the carbon 1s orbital upon decomposition is similar to nickelocene decomposition on the Ni(1 0 0) surface [21] and can be attributed to surface carbon that is carbidic in nature [43]. Decomposition also shifts the Ni 2p binding energies to lower values that are more consistent with Ni^0. The Ni $2p_{3/2}$ is observed at 852.1 eV and the $2p_{1/2}$ at 869.4 eV, values that are comparable to the reported values of 852.3 and 869.7 eV for nickel metal [43].

XPS intensities obtained from the annealed surface and (1) and (2) can be used to determine relative Ni and C surface concentrations of adsorbate remaining after heating to 525 K. For a full monolayer of nickelocene heated at 2 K s^{-1}, the C/Ag concentration ratio is 0.16, indicating that approximately 75% of the carbon initially adsorbed in the monolayer has been removed from the surface. A value of 0.03 is obtained for the Ni/Ag ratio, indicating a loss of approximately one-half of the monolayer value. These values give a new C/Ni concentration ratio of approximately 5.

Assuming that the only mechanism for removal of nickel from the surface during annealing experiments is through molecular nickelocene desorption and that nickel from the dissociated metallocene remains on the surface, the XPS data implies that half of the initial, molecularly adsorbed monolayer desorbs, while half decomposes to adsorbed cyclopentadienyl and nickel. The carbon XPS data, then, suggest that for every two

Table 3
X-ray photoelectron binding energies of $NiCp_2$ adsorbed on Ag(1 0 0) and other related species

	25 L $NiCp_2$ on Ag(1 0 0) (eV)	10 L $NiCp_2$ on Ag(1 0 0) (eV)	Annealed to 525 K (eV)	Ni metal[a] (eV)
C 1s	284.6	284.6	283.9	
Ni $2p_{3/2}$	854.6	854.6	852.1	852.3
Ni $2p_{1/2}$	871.7	871.7	869.4	869.7

[a] Data from Ref. [43].

adsorbed Cp rings, one dehydrogenates to yield hydrogen for hydrogenation of the remaining ring to cyclopentadiene and H_2 in agreement with the stoichiometry of the Cp disproportionation reaction. The desorption and decomposition of nickelocene on Ag(1 0 0) can be summarized by the following:

$$2NiCp_{2(g)} \xrightarrow{175\ K} 2NiCp_{2(ads)}$$
$$\xrightarrow{225\ K} NiCp_{2(g)} + Ni_{ads} + 2C_5H_{5(ads)}$$
$$\xrightarrow{525\ K} Ni_{(ads)} + C_5H_{6(g)} + H_{2(g)} + 5C_{(ads)}$$

where a subscript (g) indicates a gas phase species, and a subscript (ads) indicates an adsorbed species.

4. Discussion

Molecular physisorption of nickelocene on the Ag(1 0 0) substrate at 175 K is indicated by both XPS and HREELS data in agreement with previous observations [7, 17, 19–21]. The HREEL spectrum of long nickelocene exposures for the Ag(1 0 0) substrate, > 20 L, result in bilayer to multilayer adsorption with the molecular axis canted with respect to the surface normal. HREEL spectra of submonolayer to monolayer coverages show that the metallocene adsorbs with its molecular axis perpendicular to the surface.

The transition from an upright packing arrangement at monolayer and submonolayer coverages to a tilted one at higher coverages has been postulated previously [19], and is confirmed with the present data. However, we cannot distinguish between the case where the monolayer remains upright and the second layer adsorbs tilted relative to the first layer and the surface normal and one in which the formation of the second layer causes a phase transition in which both monolayer and the second layer are tilted. We postulate that the former is most likely to occur because the nickelocene most favorably interacts with the Ag(1 0 0) substrate through the π-electrons of the aromatic Cp ligand ring, keeping it up-right to maximize overlap in an η^5-Cp configuration, whereas the second layer interacts most favorably with the metallocene monolayer through forces that include Ni–Cp intermolecular interactions to give the herring-bone type packing observed for the bulk crystal structure [25].

Even at very low substrate temperatures, some decomposition of the metallocene occurs for submonolayer surface concentrations of < 0.5 ML. This decomposition is not seen for higher concentrations unless the surface is heated to ~225 K. Since nickelocene decomposition produces two Cp free-ligand adsorbates and one nickel for every molecularly adsorbed nickelocene molecule, the decomposing material will need additional surface adsorption sites. The availability of free, adjacent surface sites most likely limits the amount of decomposition that can occur at low temperatures. Above 0.5 ML, the metallocene must decompose through a displacement of adjacent molecular adsorbate, which is not observed at a significant rate below 225 K during the 1–2 h timescale of the HREELS and XPS experiments.

Three distinct desorption maxima of molecular nickelocene are observed in TPD spectra. The first, occurring initially at 210 K (peak A), is attributed to desorption of nickelocene from layers beyond the first monolayer because of its lack of saturation with increasing coverage and its zero-order behavior (Figure 6). It is clear from the lack of molecular desorption of nickelocene at sufficiently low coverages, that decomposition is more favorable than desorption when vacant adsorption sites are present and heating rates are sufficiently slow. Molecular desorption of nickelocene at 225 K (peak B) is attributed to desorption through displacement of decomposing metallocene from a surface with insufficient available adsorption sites for decomposition to occur. At 255 K, (peak C) regular molecular desorption is observed, provided some molecular metallocene survives the surface decomposition pathway.

Decomposition of adsorbed nickelocene on Ag(1 0 0) is also indicated in the cyclopentadienyl HREEL spectra observed for samples annealed at 225 K or higher. The adsorbed free-ligand Cp disproportionates to cyclopentadiene, which desorbs, and carbon fragments, which remain on the Ag(1 0 0) substrate surface. H_2 produced in the cyclopentadienyl fragmentation co-desorbs with the

cyclopentadiene at ~525 K. The first-order desorption kinetics of peak D and the co-desorption of the hydrogen indicate that a single event, most likely dehydrogenation of the free-ligand cyclopentadienyl adsorbate, activates the disproportionation reaction:

$$C_5H_{5\,ads} \overset{500\ K}{\rightarrow} C_5H_{4\,ads} + H_{ads}$$

$$C_5H_{5\,ads} + H_{ads} \overset{rapid}{\rightarrow} C_5H_{6\,g}$$

$$C_5H_{4\,ads} \overset{rapid}{\rightarrow} C_xH_y + H_{ads}$$

$$2H_{ads} \overset{rapid}{\rightarrow} H_{2\,g}$$

Fragmentation of the cyclopentadienyl on the surface represents a number of complex, but rapid, steps the final result of which is surface carbide. Nickel metal also remains on the surface at the end of the TDS process.

5. Conclusions

Nickelocene adsorbs molecularly on Ag(1 0 0) and desorbs at 255 K for molecules within the first monolayer and ~210 K for multilayers. Monolayer adsorbates are up-right, with the molecular axis along the surface normal; however, bilayer and higher multilayers present a tilted molecular geometry. For coverages of < 0.5 ML some decomposition to Cp_{ads} and Ni_{ads} is also observed even at temperatures as low as 140 K.

For $NiCp_{2\,ads}$ coverages $\gtrsim$ 0.5 ML, only molecular adsorption is detected at 175 K, but decomposition of a portion of the molecularly adsorbed metallocene occurs at higher temperatures. HREELS and TPD indicate that adsorbed nickelocene metal–ligand bond breakage begins at approximately 225 K for these higher coverages and the decomposition is accompanied by molecular desorption through displacement by the cyclopentadienyl fragments. Molecular desorption occurs at 225 K only if insufficient vacant surface sites are present to accommodate the additional metallocene fragments, for example when the surface is saturated with nickelocene and/or adsorbed cyclopentadienyl and nickel. Disproportionation of adsorbed cyclopentadienyl on Ag(1 0 0) begins at ~400 K, and reaches a maximum at ~525 K. This results in desorption of molecular hydrogen and the Cp_{ads} hydrogenation product, cyclopentadiene, as well as residual carbon and nickel-surface species.

Acknowledgements

The authors gratefully acknowledge support from the AFOSR under grant no. F49620-98-1-0463, the Petroleum Research Foundation ACS-PRF 31708AC, the NSF under CHE-9616690, and the University of Nebraska Center for Materials Research and Analysis.

References

1. J. C. Johnson. *Metallocene Technology*, Noyes Data Corporation, Park Ridge, NJ (1973).
2. D. Welipitiya, P. A. Dowben, J. Zhang, W. W. Pai and J. F. Wendelken. *Surf. Sci.* **367** (1996), p. 20.
3. D. Welipitiya, Y. L. He, J. Zhang, P. I. Oden, T. Thundat, R. J. Warmack, I. Gobulukoglu, Z. S. Shan, D. J. Sellmeyer and P. A. Dowben. *J. Appl. Phys.* **80** (1996), p. 1867.
4. G. T. Stauf, D. C. Driscoll, P. A. Dowben, S. Barfuss and M. Grade. *Thin Solid Films* **153** (1987), p. 421.
5. G. T. Stauf and P. A. Dowben. *Thin Solid Films* **156** (1988), p. L31.
6. D. Welipitiya, A. Green, J. P. Woods, P. A. Dowben, B. W. Robertson, D. Byun and J. Zhang. *J. Appl. Phys.* **79** (1996), p. 8730.
7. D. Welipitiya, C. Waldfried, C. N. Borca, P. A. Dowben, N. M. Boag, H. Jiang, I. Gobulukoglu and B. W. Robertson. *Surf. Sci.* **418** (1998), p. 466.
8. L. M. Dyagileva. *Russ. J. Phys. Chem.* **67** (1993), p. 1194.
9. F. Thibaudau, J. R. Roche and F. Salvan. *Appl. Phys. Lett.* **64** (1994), p. 523.
10. J. V. Armstrong, A. A. Burk, Jr., J. M. D. Coey and K. Moorjani. *Appl. Phys. Lett.* **50** (1987), p. 1231.
11. W. W. Pai, J. Zhang, J. F. Wendelken and R. J. Warmack. *J. Vac. Sci. Technol. B* **15** (1997), p. 785.
12. L. Brissonneau and C. Vahlas. *Chem. Vap. Depos.* **5** (1999), p. 135.
13. L. Brissonneau, D. de Caro, D. Boursier, R. Madar and C. Vahlas. *Chem. Vap. Depos.* **5** (1999), p. 143.
14. L. Brissonneau, A. Reynes and C. Vahlas. *Chem. Vap. Depos.* **5** (1999), p. 281.
15. L. Brissonneau, A. Reynes and C. Vahlas. *J. Phys. IV France* **9** (1999), p. 57.

16. D. de Caro, L. Brissonneau, D. Boursier, R. Madar and C. Vahlas. *J. Phys. IV France* **9** (1999), p. 1099.
17. D. Welipitiya, C. N. Borca, C. Waldfried, C. Hutchings, L. Sage, C. M. Woodbridge and P. A. Dowben. *Surf. Sci.* **393** (1997), p. 34.
18. R. Zanoni, M. N. Piancastelli, M. Marsi and G. Margartondo. *J. Electron. Spectrosc. Rel. Phenom.* **57** (1991), p. 199.
19. C. N. Borca, D. Welipitiya, P. A. Dowben and N. M. Boag. *J. Phys. Chem. B* **104** (2000), p. 1047.
20. D. L. Pugmire, C. M. Woodbridge and M. A. Langell. *Surf. Sci.* **411** (1998), p. L844.
21. D. L. Pugmire, C. M. Woodbridge, S. Root and M. A. Langell. *J. Vac. Sci. Technol. A* **17** (1999), p. 1581.
22. C. Waldfried, D. Welipitiya, C. W. Hutchings, H. S. V. de Silva, G. A. Gallup, P. A. Dowben, W. W. Pai, J. Zhang, J. F. Wendelken and N. M. Boag. *J. Phys. Chem. B* **101** (1997), p. 9782.
23. E. R. Lippincott and R. D. Nelson. *Spectrochim. Acta* **10** (1958), p. 307.
24. K. Chhor, G. Lucazeau and C. Sourisseau. *J. Raman Spectrosc.* **11** (1981), p. 183.
25. P. Seiler and J. D. Dunitz. *Acta Cryst. B* **36** (1980), p. 2255.
26. M. Barber, J. A. Connor, L. M. R. Derrick, M. B. Hall and I. H. Hillier. *J. Chem. Soc. Farad. Trans. II* **69** (1973), p. 559.
27. J. H. Scofield. *J. Electron. Spectrosc. Relat. Phenom.* **8** (1976), p. 129.
28. D. Briggs, M. P. Seah, Practical Surface Analysis, vol. 1, second ed., Wiley, New York, 1990 (Chapter 5).
29. C. M. Woodbridge, D. L. Pugmire, R. C. Johnson, N. M. Boag and M. A. Langell. *J. Phys. Chem. B* **104** (2000), p. 3085.
30. F. A. Cotton and G. Wilkinson. In: *Advanced Inorganic Chemistry*, Wiley, New York (1972), p. 120.
31. D. R. Penn. *J. Electron. Spectrosc. Relat. Phenom.* **9** (1976), p. 29.
32. M. A. Langell, C. L. Berrie, M. H. Nassir and K. W. Wulser. *Surf. Sci.* **320** (1994), p. 25.
33. G. A. Somorjai. *Introduction to Surface Chemistry and Catalysis*, Wiley, New York (1994).
34. W. H. Gries. *Surf. Int. Anal.* **24** (1996), p. 38.
35. M. X. Yang, S. K. Jo, A. Paul, L. Avila, B. E. Bent and K. Nishikida. *Surf. Sci.* **325** (1995), p. 102.
36. L. A. Torres-Gomez, G. Barreiro-Rodriguez, F. Mendez-Ruz, Thermochimica Acta 124 (1988) 179.
37. W. W. Pai, Z. Zhang, J. Zhang and J. F. Wendelken. *Surf. Sci.* **393** (1997), p. L106.
38. N. R. Avery. *J. Electron. Spectrosc. Rel. Phenom.* **39** (1986), p. 1.
39. National Institute of Standards, Technology (NIST) Standard Reference Database Number 69, Feb. 2000, NIST Chemistry WebBook (http://webbook.nist.gov/chemistry/).
40. P. T. Sprunger and E. W. Plummer. *Phys. Rev. B* **48** (1993), p. 14436.
41. G. Lee and E.W. Plummer. *Phys. Rev. B* **51** (1995), p. 7250.
42. P. A. Redhead. *Vacuum* **12** (1962), p. 203.
43. G. E. Muilenberg (Ed.), Handbook of X-Ray Photoelectron Spectroscopy, Perkin–Elmer Corporation, Eden Prairie, Minnesota, 1979.